nature geoscience

SUPPLEMENTARY INFORMATION

https://doi.org/10.1038/s41561-019-0315-9

In the format provided by the authors and unedited.

Increased landslide activity on forested hillslopes following two recent volcanic eruptions in Chile

Oliver Korup[1,2]*, Jan Seidemann[1] and Christian H. Mohr[1]

[1]Institute of Environmental Science and Geography, University of Potsdam, Potsdam, Germany. [2]Institute of Geosciences, University of Potsdam, Potsdam, Germany. *e-mail: oliver.korup@geo.uni-potsdam.de

Increased landslide activity on forested hillslopes following two recent volcanic eruptions in Chile

Oliver Korup[1,2*], Jan Seidemann[1], Christian H. Mohr[1]

[1]Institute of Environmental Science and Geography, University of Potsdam, Germany

[2]Institute of Geoscience, University of Potsdam, Germany

*Corresponding author (oliver.korup@geo.uni-potsdam.de)

Supplementary Information

Rainfall data. The conditions for rainfall-triggered landslides can be approximated by critical values of rainfall intensity, duration, and totals at which slope failure occurred[S1,S2]. To check whether the landslides that we mapped were linked to spells or periods of high rainfall instead of tephra deposition, we compiled and analysed freely accessible daily rainfall data from ten climate stations[S3] within a 100-km radius of Chaitén and Puyehue volcanoes (Figure S1). Some close-by candidate rain gauges had many missing records, so that we used the most complete 15-year periods roughly centred on the eruption dates (Figures S2, S3).

Figure S1. Map of ten rain gauges (http://www.cr2.cl/datos-de-precipitacion/) within 100 km of Chaitén and Puyehue volcanoes, southern Chile. Shaded topography taken from SRTM digital elevation data (https://www2.jpl.nasa.gov/srtm/).

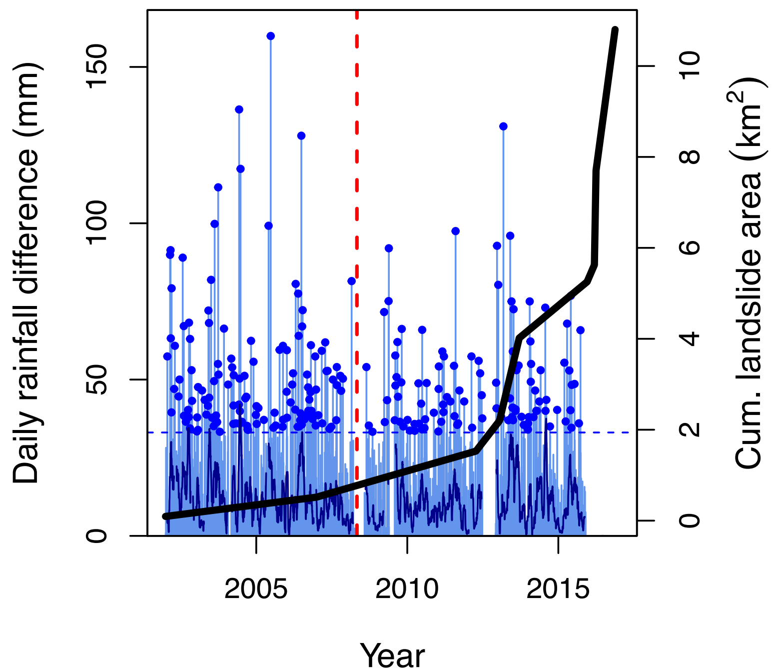

Figure S2. Differences in daily rainfall (medium blue bars) as a proxy of rainfall intensity at Puerto Cárdenas, SSE of Chaitén volcano. Dark blue jagged line is 28-day centred running mean and highlights seasonal cycles. Horizontal dashed line is 95th percentile, and blue circles mark values above this threshold. Vertical red dashed line marks eruption date of Chaitén volcano, and black thick line is estimated cumulative landslide area mapped from satellite images. Note the two major data gaps, the first around the time of the eruption.

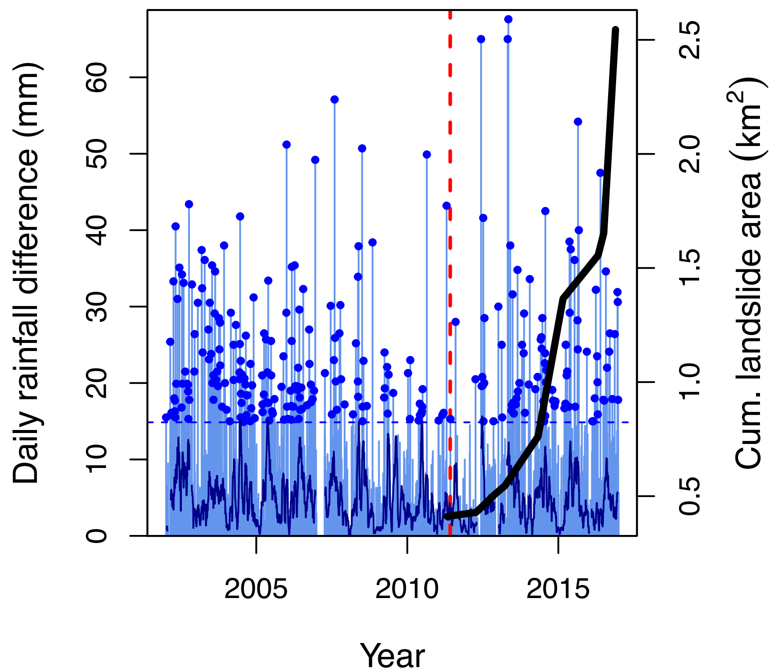

Figure S3. Differences in daily rainfall (medium blue bars) as a proxy of rainfall intensity at Futacuhuin, WSW of Puyehue volcano. Dark blue jagged line is 28-day centred running mean and highlights seasonal cycles. Horizontal dashed line is 95th percentile, and blue circles mark values above this threshold. Vertical red dashed line marks eruption date of Puyehue volcano, and black thick line is estimated cumulative landslide area mapped from satellite images.

Apart from using the raw daily rainfall data [mm], we also computed the differences in daily rainfall [mm] and their 95th percentiles to capture high-intensity storms; rainfall totals [mm] separated by at least one day without rain; and the number of consecutive days with and without rain. We used a Bayesian robust linear regression with η = 10 degrees of freedom (see Methods) to estimate trends in daily rainfall; the 95th percentile of differences in daily rainfall; rainfall totals separated by at least one dry day; and the consecutive number of days with and without rain for each station between 2002 and 2017.

We find that all stations reveal either no credible trends (in the Bayesian sense, and analogous to 'statistically significant' in frequentist statistics) or weak, though credible, negative trends in these rainfall characteristics; the only exception is that most stations show a credible positive trend in the number of consecutive days without rain (Tables S1, S2).

Table S1. Trends of rainfall data at gauges near Chaitén and Puyehue volcanoes, southern Chile, between 2002 and 2017. We estimated the trends from a Bayesian robust linear regression with η = 10 degrees of freedom of (a) daily rainfall [mm], and (b) the number of consecutive days without rain, as a function of time. We summarise the posterior distributions of the slopes from this robust regression using their 95% highest density intervals. Grey shades mark posterior trends that are indistinguishable from zero with 95% probability.

Station	Location	Length of record [d]	95% HDI of trend in daily rainfall [mm/d]		95% HDI of trend in consecutive days without rain [1/d]	
Lago Maihue	40.2172°S 72.1492°W	5477	-4.11×10^{-4}	-9.40×10^{-5}	-2.65×10^{-5}	6.04×10^{-5}
Lago Ranco	40.3172°S 72.4692°W	5441	-3.07×10^{-4}	-6.41×10^{-5}	-7.81×10^{-6}	7.99×10^{-5}
Anticura	40.6553°S 72.1844°W	2581	-3.41×10^{-4}	-3.92×10^{-5}	2.49×10^{-5}	1.32×10^{-4}
Futacuhuin	40.7231°S 72.4400°W	5319	-2.37×10^{-4}	-3.13×10^{-5}	6.20×10^{-5}	1.35×10^{-4}
Lago Chapo	41.4172°S 72.5958°W	4879	-4.68×10^{-4}	-4.22×10^{-5}	-1.04×10^{-5}	4.63×10^{-5}
Pto. Montt	41.4600°S 72.9378°W	5479	-4.29×10^{-4}	-2.07×10^{-4}	4.83×10^{-5}	9.72×10^{-5}
Chaitén*	42.9147°S 72.7108°W	2177	-1.47×10^{-3}	1.05×10^{-4}	1.80×10^{-4}	3.92×10^{-4}
Pto. Cardenas	43.1750°S 72.4308°W	4713	-9.07×10^{-4}	-3.30×10^{-4}	8.20×10^{-5}	1.51×10^{-4}
Lago Espolon	43.2158°S 71.9306°W	5375	-5.16×10^{-4}	-1.78×10^{-4}	9.75×10^{-5}	1.93×10^{-4}
Valle Rio Frio	43.4683°S 72.3536°W	5463	-9.77×10^{-4}	-5.27×10^{-4}	1.14×10^{-4}	1.99×10^{-4}

*Rainfall records terminated with the 2008 eruption of Chaitén volcano.

Table S2. Trends of rainfall data at gauges near Chaitén and Puyehue volcanoes, southern Chile, between 2002 and 2017 (see Table S1). We estimated the trends from a Bayesian robust linear regression with η = 10 degrees of freedom of (a) the 95th percentile of daily differences in rainfall [mm]; (b) the rainfall totals [mm] per event, defined here as the number of consecutive rainy days separated by at least one day without rain; and the number of consecutive days with rain (c), all as a function of time. We summarise the posterior distributions of the slopes from this robust regression using their 95% highest density intervals. Grey shades mark posterior trends that are indistinguishable from zero with 95% probability.

Station	95% HDI of trend in 95th percentile of daily differences in rainfall [mm/d]		95% HDI of trend in rainfall totals per event [mm/d]		95% HDI of trend in consecutive days with rain [1/d]	
Lago Maihue	-6.18×10^{-4}	1.84×10^{-3}	-4.12×10^{-3}	9.02×10^{-5}	-1.35×10^{-5}	8.03×10^{-5}
Lago Ranco	-6.58×10^{-4}	8.11×10^{-4}	-3.33×10^{-3}	-2.38×10^{-5}	-1.21×10^{-4}	1.19×10^{-4}
Anticura	-3.63×10^{-4}	1.65×10^{-3}	-7.90×10^{-6}	1.80×10^{-5}	-5.88×10^{-7}	1.02×10^{-5}
Futacuhuin	-4.43×10^{-4}	6.86×10^{-4}	-1.85×10^{-3}	9.67×10^{-4}	-2.02×10^{-4}	7.30×10^{-5}
Lago Chapo	-1.52×10^{-3}	6.61×10^{-4}	-1.11×10^{-2}	-8.41×10^{-3}	-9.92×10^{-4}	-8.15×10^{-4}
Pto. Montt	-1.18×10^{-3}	1.83×10^{-4}	-3.97×10^{-3}	-4.91×10^{-4}	-3.43×10^{-4}	-3.39×10^{-5}
Chaitén*	-3.81×10^{-3}	4.25×10^{-3}	-2.63×10^{-9}	2.38×10^{-9}	-1.22×10^{-10}	1.27×10^{-10}
Pto. Cardenas	-1.90×10^{-3}	8.15×10^{-4}	-1.78×10^{-9}	1.69×10^{-9}	-6.46×10^{-4}	-4.76×10^{-4}
Lago Espolon	-1.34×10^{-3}	0.64×10^{-4}	-2.12×10^{-3}	1.98×10^{-3}	-9.76×10^{-5}	7.85×10^{-5}
Valle Rio Frio	-7.94×10^{-4}	8.59×10^{-4}	-6.44×10^{-3}	-5.67×10^{-5}	-2.38×10^{-4}	1.90×10^{-5}

*Rainfall records terminated with the 2008 eruption of Chaitén volcano.

We infer from these trend estimates that local and regional rainfall totals, duration, and daily changes remained comparable in the years before and after the eruptions of Chaitén and Puyehue volcanoes; if anything, conditions became slightly drier. The distribution of rainfall intensity that we estimated with the 95th percentile of daily differences in rainfall is similar before and after the eruptions (Figures S2, S3), revealing no obvious change in the pattern of high-intensity rainstorms.

We emphasise that this rainfall analysis is only broadly informative, as the exact timing of the landslides that we mapped from satellite images remain elusive. Most of the rain gauges are below 350 m a.s.l., and may not capture topographic effects on rainfall in the Patagonian fjords, or possible local thermal or chemical atmospheric disturbances during and after the volcanic eruptions. Yet we find it highly plausible that the landslides studied were triggered during or shortly after rainstorms, especially in the absence of any major earthquakes during our study period. Rain-on-snow or rapid snowmelt events could be other candidates for triggering the post-eruptive landslides, but the clustered distribution of slope failures in the wind shadows close to the volcanoes requires that this trigger be very localised. Higher heat flux near the volcanoes may have caused more winter precipitation to fall as rain. In any case, we recall that our study focuses on the causes (tephra deposition and tree dieback), instead of the triggers (most likely rainfall), of these post-eruptive landslides.

Landslide data. We used freely available LANDSAT and Sentinel-2 satellite imagery (https://earthexplorer.usgs.gov/, https://sentinel.esa.int/) to map landslides before and after the eruptions of Chaitén and Puyehue volcanoes (see Methods, Table S3). Judging from time series of individual landslides, we found that fresh scars remained visible for at least ten years as bright patches in the otherwise dark green rainforest. We therefore assumed that the earliest landslides that we mapped from 2001 imagery date back into the 1990s at least.

Table S3. Satellite images used for landslide mapping around Chaitén and Puyehue volcanoes. We also used satellite images and high-resolution air photo from a digital globe (https://www.google.com/intl/de/earth/) for systematic cross-checks. Where cloud cover or image boundaries limited our mapping, we merged the results from images in close temporal succession, and used the mean date as the time stamp.

Satellite image ID	Resolution [m]	Date
Chaitén		
LE07_L1TP_232090_20011208_20170202_01_T1	30	08 Dec 2001
E07_L1TP_232090_20040319_20170121_01_T1	30	19 Mar 2004
LT05_L1TP_232090_20050125_20161127_01_T1	30	25 Jan 2005
LE07_L1TP_232090_20070107_20170105_01_T1	30	07 Jan 2007
LE07_L1TP_233090_20110210_20161211_01_T1	30	10 Feb 2011
LE07_L1TP_232090_20120410_20161203_01_T1	30	10 Apr 2012
LE07_L1TP_232090_20120121_20161203_01_T1	30	21 Jan 2013
LC08_L1TP_232090_20130928_20170502_01_T1	30	28 Sep 2013
LC08_L1TP_232090_20151105_20170402_01_T1	30	05 Nov 2015
LC08_L1TP_233089_20160131_20170330_01_T1	30	31 Jan 2016
LE07_L1TP_232090_20160201_20161015_01_T1	30	01 Feb 2016
LC08_L1TP_232090_20161107_20170318_01_T1	30	07 Nov 2016
S2A_MSIL1C_20170317T144401_N0204_R053_T18GYT_20170317T144357	10	17 Mar 2017
S2A_MSIL1C_20170317T144401_N0204_R053_T18GXT_20170317T144357	10	17 Mar 2017
S2A_MSIL1C_20170416T142751_N0204_R053_T18GYT_20170416T143935	10	16 Apr 2017
S2A_MSIL1C_20170416T142751_N0204_R053_T18GXT_20170416T143935	10	16 Apr 2017
S2A_MSIL1C_20170320T143741_N0204_R096_T18GYT_20170320T145159	10	20 Mar 2017
S2A_MSIL1C_20170320T143741_N0204_R096_T18GXT_20170320T145159	10	20 Mar 2017
S2A_MSIL1C_20170205T142851_N0204_R053_T18GYT_20170205T144421	10	05 May 2017
S2A_MSIL1C_20170205T142851_N0204_R053_T18GXT_20170205T144421	10	05 May 2017
Puyehue-Cordón Caulle		
LE07_L1TP_233088_20030409_20170126_01_T1	30	09 Apr 2003

LE07_L1TP_232088_20080314_20161230_01_T1	30	14 Mar 2008
LE07_L1TP_232088_20091128_20161219_01_T1	30	14 Dec 2009
LE07_L1TP_233088_20110501_20161210_01_T1	30	01 May 2011
LT05_L1TP_232088_20111025_20161005_01_T1	30	25 Oct 2011
LE07_L1TP_233088_20120213_20161203_01_T1	30	13 Feb 2012
LE07_L1TP_232088_20121104_20161129_01_T1	30	04 Nov 2012
LE07_L1TP_232088_20130328_20161124_01_T1	30	28 Mar 2013
LC08_L1TP_233088_20130412_20170505_01_T1	30	12 Apr 2013
LC08_L1TP_232088_20131030_20170429_01_T1	30	30 Oct 2013
LC08_L1TP_232088_20140323_20170424_01_T1	30	23 Mar 2014
C08_L1TP_232088_20150222_20170412_01_T1	30	22 Feb 2015
LC08_L1TP_232088_20151105_20170402_01_T1	30	05 Nov 2015
LE07_L1TP_232088_20160304_20161014_01_T1	30	04 Mar 2016
LC08_L1TP_232088_20160616_20170324_01_T1	30	16 Jun 2016
LE07_L1TP_233088_20161122_20170113_01_T1	30	22 Nov 2016

In the field we measured in detail the geometry of 15 post-eruptive landslides around Chaitén volcano from photogrammetric unmanned aerial vehicle (UAV) surveys (see Methods). At six additional landslides close to roads or footpaths we used a measuring tape and an inclinometer to randomly check local landslide scar and deposit depths. At none of these sites did we find deposits thicker than about 2 m. From the UAV surveys, we obtained full-colour orthophoto mosaics that we sampled to a nominal pixel resolution of 0.125 m, and digital elevation models with a nominal pixel resolution of 0.25 m. We computed and superimposed 1-m contours to visually enhance the orthophotos that we draped over the hillshaded digital topography, and to aid landslide mapping at a maximum scale of 1:100 (Figure S4).

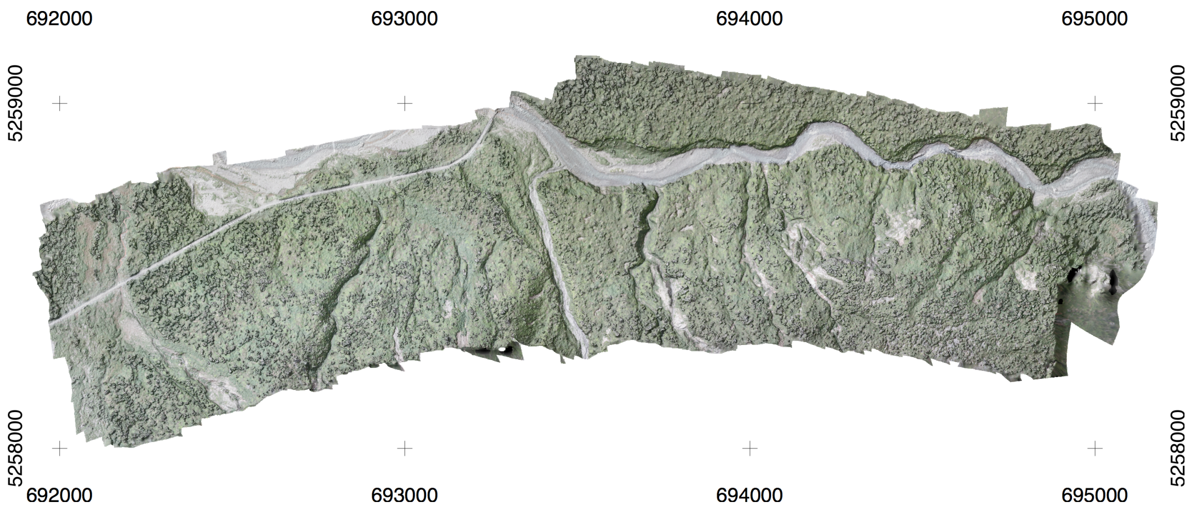

Figure S4. Orthophoto derived from an eBee RTK unmanned aerial vehicle of Rayas River on the NE slopes of Chaitén volcano, February 2018. Coordinates refer to UTM zone 18S; spacing of crosses is 1 km. We used a photogrammetric analysis (structure-from-motion) to generate a digital elevation raster with 0.25 m nominal resolution. Bright hairpin-shaped patches in the lower right of the image are shallow post-eruptive landslides.

We chose this scale to avoid mapping spurious details or noise arising from local pixel errors. We did not correct the elevation data for effects of forest vegetation that in the landslide scars especially enhanced or exaggerated the local surface changes due to slope failure. Hence, we refrained using any automatic cut-and-fill methods to estimate landslide volumes and manually mapped footprint planform areas first. In a next step we approximated the former ground surface in landslide scar and deposit areas by connecting with straight lines the intersection of contour lines with the landslide outline. This approach simplistically assumes a planar ground surface prior to slope failure, but is the most objective and reproducible approach for estimating mean scar and deposit depth per contour (Figure S5).

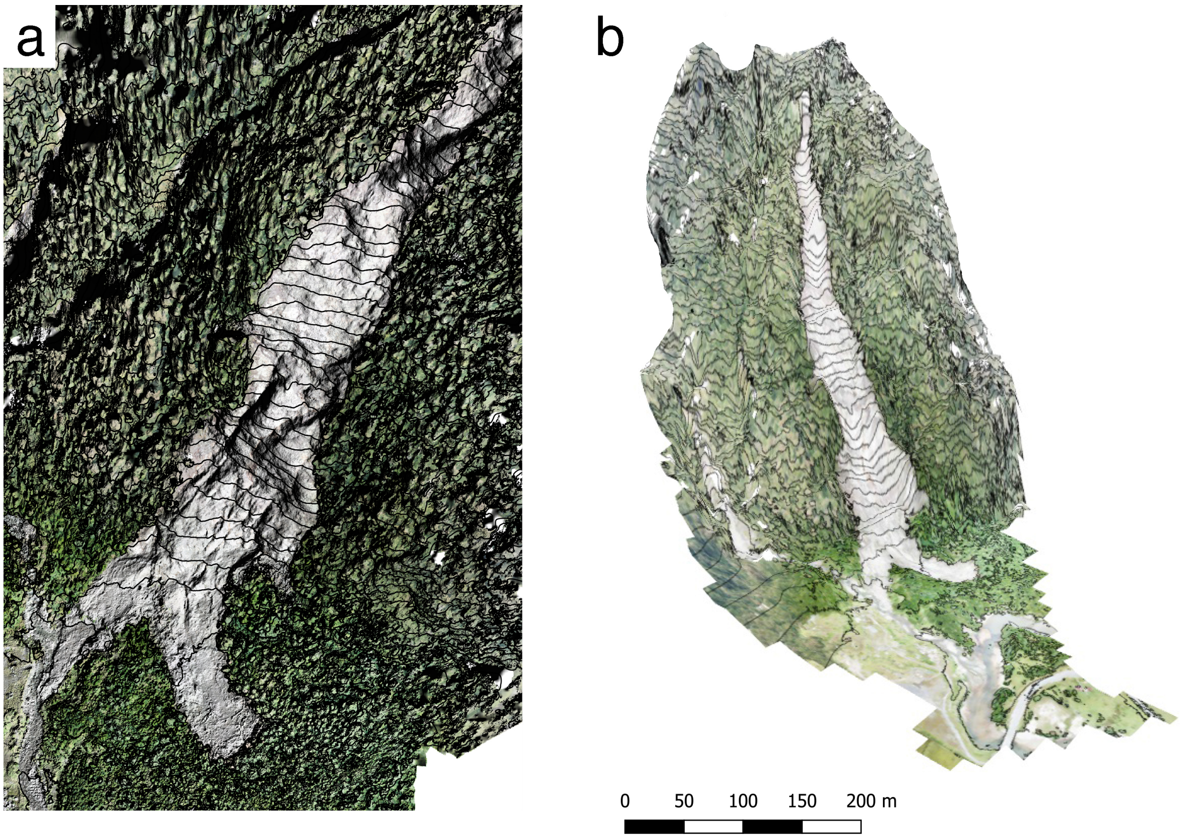

Figure S5 a. Example of an orthophoto mosaic derived from an UAV survey of a shallow soil/debris landslide (bright) in dense rainforest (dark) ~8 km south of Chaitén volcano (Figure 5b). b. Contrast-adjusted orthophoto draped over a digital elevation model obtained via structure-from-motion photogrammetry using a dense point cloud interpolation. Contour spacing is 10 m for clarity, although we used 1-m contours for landslide mapping, based on a nominal 0.25-m raster resolution. The original pixel resolution of the orthophoto was 0.07 m. Total vertical drop height of the landslide is 480 m.

We estimated the total landslide volume by adding up these individual sliced estimates; where possible we measured both scars and deposits (Table S4). From independent repeat digital mapping we estimate a mean relative error in landslide area of the order of +/– 5%.

Table S4. Estimated landslide footprint areas and volumes derived from photogrammetric UAV surveys in the vicinity of Chaitén volcano, February 2018. Areas were obtained by repeatedly digitizing the high-contrast outlines of highly reflective landslide scars and deposits that stood out from the surrounding dark vegetation in high-resolution orthophoto mosaics. Coordinates are for UTM zone 18S and approximately locate the landslide head scarps. Volume type refers to estimates of either the entire landslide scar and deposit ('Total') or only the scar area ('Scar'). We rounded all figures eventually to avoid spurious volumetric estimates.

Landslide code	Coordinates UTM 18S	Estimated area [m^2]	Estimated volume [m^3]	Volume type
Blanco_DG*	690277W 524960S	270190	200000	Total
Chaitén_ls1*	693215W 5257612S	3870	714	Total
Chaitén_ls1	693215W 5257612S	1040	673	Scar
Chaitén_ls2	689203W 5254647S	688	69	Total
Chaitén_ls2	689203W 5254647S	320	204	Scar
Rayas_ls1	693361W 5258437S	301	140	Total
Rayas_ls1	693361W 5258437S	102	48	Scar
Rayas_ls2	693117W 5258376S	748	614	Total
Rayas_ls2	693117W 5258376S	275	359	Scar
Rayas_ls3	694333W 5258482S	706	1529	Scar
Rayas_ls4	694833W 5258458S	3971	4551	Scar
Rayas_ls5	694646W 5258425S	713	486	Scar

Rayas_ls6	694439W 5258587S	359	505	Scar
Rayas_ls7	694463W 5258606S	96	37	Scar
Rayas_ls8	693904W 5258596S	248	137	Scar
Rayas_ls9	694272W 5258476S	1962	610	Total
Rayas_ls9	694272W 5258476S	245	147	Total
Rayas_ls10	694215W 5258550S	1513	958	Total
Rayas_ls11	694239W 5258646S	88	77	Scar
Chaitén_ls12	694145W 5258374S	301	121	Total

*Estimate partly augmented by local field measurements.

Volcanoes and forest cover in Chilean Patagonia. To estimate to first order the regional long-term relevance of post-eruptive landslides in forests killed or damaged by tephra, we compiled published data on explosive eruptions in the Andean Southern Volcanic Zone (SVZ) of Chile[S4]. Maps of reconstructed tephra thickness from Late Glacial to Holocene eruptions show that most of the land area in the Patagonian fjords between 41°S and 46°S had fallout of at least 0.1 m (Figure 11 in ref. S4). Most post-eruptive landslides around Chaitén and Puyehue volcanoes detached where tephra was 0.05-0.2 m thick, so that 0.1-m isopachs might roughly delineate focus areas of post-eruptive slope instability. At least eleven eruptions with an estimated Volcanic Explosivity Index (VEI) of 4.5 to 5.5 occurred in the past 10,500 years, covering more than 10,260 km^2 beneath >0.1 m of tephra (Tables 4, 5 in ref. S4). Based on 53 documented eruptions with VEI > 3 since Late Glacial times, we estimate a recurrence interval of <275 years (ref. 8). However, a local study[S5] of 26 tephra layers preserved in a lake near Chaitén identified many more eruptions from this and nearby Minchinmávida volcano, and proposed a median recurrence interval of 310 years from both sources in the past 10,000 years; eruptions of Chaitén volcano alone had a median recurrence interval of 200 years in the past millennium.

To estimate the impacts of explosive eruptions on rainforests in the region, we estimated the percentage of tree and water cover around

(a) 56 volcanoes that were active in the Holocene between 35°S and 55°S; and

(b) 19 volcanoes between 41°S and 46°S (including Puyehue and Chaitén), which is a segment with a detailed eruption history[S4].

We used a 30-km radius around each volcano; this radius captured most of the post-eruptive landslide activity linked to forest dieback around Chaitén and Puyehue volcanoes, and also roughly approximates the average distance between most neighbouring volcanoes.

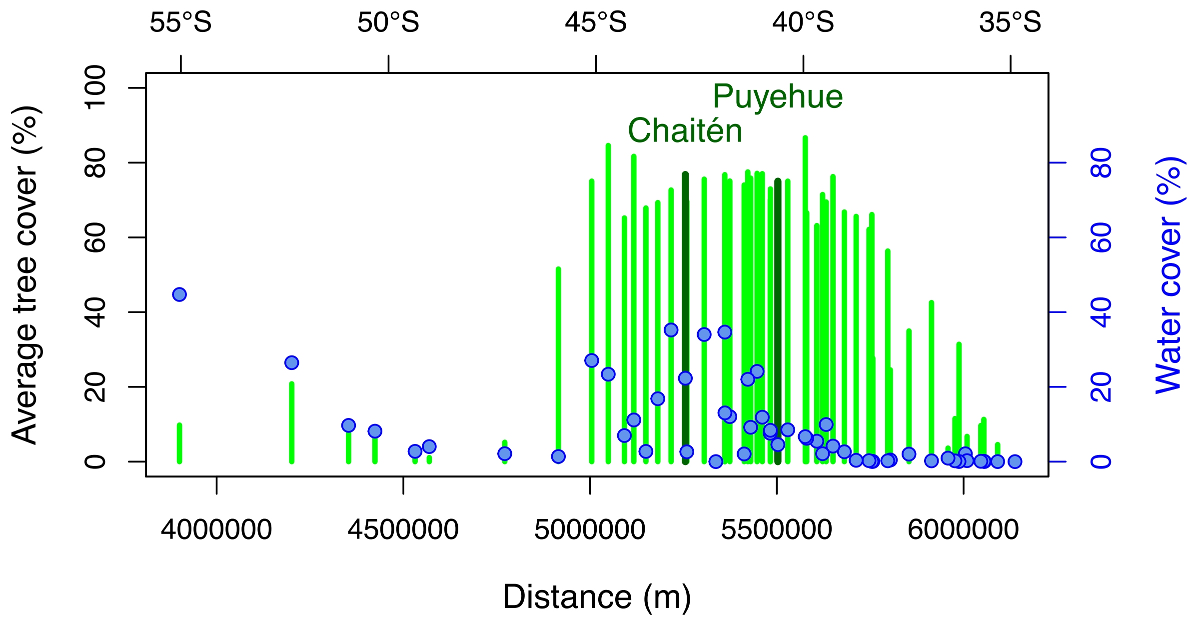

Figure S6. Area-weighted average tree and water cover [%] within 30 km of each of 56 Andean volcanoes that had been active in the Holocene. Tree cover (green bars) is averaged over all pixels in this circular area that had a normalised difference vegetation index (NDVI) indicative of forest[18] in the year 2000; percentage of water cover (blue circles) is from the same study[18]. Distance scale is in coordinates of UTM zone 18S.

We find that, within 30 km of each of the 56 Andean volcanoes, mean area-weighted tree cover[18] was 48 $^{+}/_{-}$ 4% (and 69 $^{+}/_{-}$ 4% between 41°S and 46°S) in the year 2000 (Figure S6; $^{+}/_{-}$ refers to standard errors of the means). This tree cover estimate is corrected for the many fjords and lakes south of 39°S in particular. On average 9 $^{+}/_{-}$ 1% of the area within 30 km of each volcano is covered by water; between 41°S and 46°S this average water cover is 16 $^{+}/_{-}$ 3%, so that sediments and biomass mobilised after volcanic disturbance have short transport distances to fjords and lakes.

For estimating regional rates of organic carbon erosion following explosive eruptions, we consulted published data from temperate rainforests (Table S5). Undisturbed Andean forests at ~37°S have an above-ground biomass of 50-64 tC ha^{-1}, and 2.7 to 3.5 times more soil organic carbon (OC)[S6]. *Nothofagus antarctica* forests have an average live biomass of about 84 tC ha^{-1}, and their soils can have up to twice as much OC[S7]. Given the much higher carbon stock estimates for temperate rainforests between 41°S and 46°S, we conservatively assume a minimum average forest biomass of 100 tC ha^{-1} (200 t C ha^{-1}) between 35°S and 55°S (41°S and 46°S).

Table S5. Reported average organic carbon (OC) stocks in temperate rainforests estimated from field-based (plot-scale) studies.

Location	OC stock [tC ha^{-1}]	Description	Ref.
Southern Patagonia, Chile	40-153	Live tree biomass of *Nothofagus antarctica* stands, partly model-based	S7
E Twin Creek, B.C., Canada	388	Total forest stock, uncut old growth inland temperate rainforest	S8
Lunate Creek, B.C., Canada	574	Total forest stock, uncut old growth inland temperate rainforest	S8
Minnow Creek, B.C., Canada	402	Total forest stock, uncut old growth inland temperate rainforest	S8
Chiloé, Chile	58-76	Large woody debris, selectively logged old growth temperate rainforest	S9
Chiloé, Chile	180-381	Large woody debris, gap-phase dynamics in old growth temperate rainforest	S9
New Zealand (averaged over plots)	132	Total forest ecosystem stock of 25-year old *Nothofagus solandri* var. *cliffortioides*	S10
New Zealand (averaged over plots)	230	Total forest ecosystem stock of 125-year old *Nothofagus solandri* var. *cliffortioides*	S10
Craigieburn Range, New Zealand	152-219	Total forest stock of 125- to >150-year old, partly disturbed, *Nothofagus solandri* var. *cliffortioides*	S11
Craigieburn Range, New Zealand	114	Total forest stock of 25-year old sapling stands of *Nothofagus solandri* var. *cliffortioides*	S11

Chile (averaged over plots)	877	Above-ground biomass of *Nothofagus*-dominated forests	S12
Chile (averaged over plots)	89	Large woody debris in *Nothofagus*-dominated stands	S12
Chiloé, Chile	446-554	Above-ground biomass of North Patagonian rainforest	S13
Chiloé, Chile	384-602	Above-ground biomass of Valdivian rainforest	S13
Chaitén, Chile	370	Total floodplain forest biomass	8

In total, we estimate that at least 0.44 Gt C of forest biomass is within 30 km of the 56 volcanoes. Multiplying the assumed minimum forest biomass of 100 tC ha^{-1} (200 tC ha^{-1}) by the local average tree cover, we estimate to first order that forests within 30 km of a given volcano store 12.1 $^{+}/_{-}$ 7.7 Mt C on average ($^{+}/_{-}$ 1 σ) in the greater region; between 41°S and 46°S, this estimate is 32.4 $^{+}/_{-}$ 8.9 Mt C. We double these estimates to account for soil OC, which we assume to be at least as much as that in the living biomass.

Assuming, for the sake of argument, that the average percentage tree cover has remained constant during the past millennia, we can estimate to first order the mean annual OC yields from post-eruptive landslides within 30 km of a given volcano, and for a specified recurrence interval. Following the eruptions of Chaitén and Puyehue, landslides mobilised roughly 1-5% of the estimated forest biomass in a 30-km radius around the volcanoes, so that we consider a range of 1-10% for estimating the local average OC yields (Table S6).

Table S6. First-order estimates of local average annual organic carbon (OC) yields from landslides following explosive eruptions in the Southern Volcanic Zone, assuming that each eruption (VEI >3) with specified recurrence interval causes forest dieback after tephra fall, and that landslides erode the specified fraction of thus killed forest. The term 'local' refers to a circle of 30-km radius around a given volcano, corrected for fjord and lake areas. See text for estimates of mean OC stocks; factor two accounts for soil organic carbon (error bars are $^{+}/_{-}$ 1 σ). Note that estimated OC yields refer to mass mobilised by landslides only, and reveal nothing about storage or eventual burial or oxidation.

Study area	Recurrence interval [yr]	Local mean OC stock in forest biomass and soil [Mt C]	Local forest eroded by post-eruptive landslides [%]	Local average OC yield [tC km^{-2} yr^{-1}]
35°S – 55°S	275	(12.1 $^{+}/_{-}$ 7.7) × 2	1	0.4 $^{+}/_{-}$ 0.2
35°S – 55°S	275	(12.1 $^{+}/_{-}$ 7.7) × 2	10	3.5 $^{+}/_{-}$ 2.2
41°S – 46°S	275	(32.4 $^{+}/_{-}$ 8.9) × 2	1	1.0 $^{+}/_{-}$ 0.3
41°S – 46°S	275	(32.4 $^{+}/_{-}$ 8.9) × 2	10	10.1 $^{+}/_{-}$ 2.6
Chaitén	310	33.7 × 2	1	1.0
Chaitén	310	33.7 × 2	10	9.9
Chaitén	200	33.7 × 2	1	1.5
Chaitén	200	33.7 × 2	10	15.4

We conservatively estimate that post-eruptive landslides may erode between 0.4 and 10 tC km^{-2} yr^{-1} on average from disturbed forests within 30 km of a given volcano in the SVZ over several millennia. We stress that OC yields were much higher in the first decade following the eruption, especially at the scale of single catchments. Landslides in the Rio Blanco catchment (77 km^{2}), which drains most of the southern flanks of Chaitén volcano, had eroded 265 $^{+}/_{-}$ 22 tC km^{-2} yr^{-1} in the first eight years after the 2008 eruption. This estimate is based on a specific landslide erosion of 4,240 $^{+}/_{-}$ 423 t km^{-2} yr^{-1}, and a mean OC content of 4.6% in deposits with a bulk density of 0.9 t m^{-3}. The resulting OC yield exceeds decadal yields from rainfall-induced landslides in temperate rainforest in the Southern Alps, New Zealand[30], and tropical cloud and rainforest in the Peruvian Andes[31]. Even if conservatively assuming a minimum soil OC content of 0.8% around Chaitén[8], we obtain a post-eruptive landslide erosion rate of 103 $^{+}/_{-}$ 3 tC km^{-2} yr^{-1}, which is still among the highest reported. Post-eruptive landslide activity similarly peaked in the first four years following the 1980 eruption of Mount St. Helens[S14], but the associated OC yields remain unknown. Given recurrence intervals of 200-300 years for explosive volcanic eruptions near Chaitén[S5], and landslide erosion similar to that following the 2008 eruption, the long-term average OC yield by post-eruptive landslides could be as high as 50-80 tC km^{-2} yr^{-1} in the Rio Blanco catchment, and thus an order of magnitude higher than our regional estimates. These estimates cannot reveal the eventual fate of the organic carbon mobilised, which may be partly stored in low-order catchments, floodplains, or river deltas, or gradually broken down and oxidised during intermittent transport. In this context, sedimentary archives in nearby fjords or lakes[S15] may be amenable for reconstructing carbon sequestration and for further constraining these rates.

Supplementary References

1. Guzzetti, F., Peruccacci, S., Rossi, M. & Stark, C. P. The rainfall intensity–duration control of shallow landslides and debris flows: an update. *Landslides* **5**, 3–17 (2005).

2. Saito, H., Korup, O., Uchida, T., Hayashi, S. & Oguchi, T. Rainfall conditions, typhoon frequency, and contemporary landslide erosion in Japan. *Geology* **42,** 999–1002 (2014).

3. Alvarez-Garreton, C. et al. The CAMELS-CL dataset: catchment attributes and meteorology for large sample studies – Chile dataset. *Hydrol. Earth Sys. Sci.*, https://doi.org/10.5194/hess-2018-23 (2018).

4. Watt, S. F. L. et al. Holocene tephrochronology of the Hualaihue region (Andean southern volcanic zone, ~42° S), southern Chile. *Quatern. Int.* **246**, 324–343 (2011).

5. Moreno, P. I. et al. A past-millennium maximum in postglacial activity from Volcán Chaitén, southern Chile. *Geology* **43**, 47–50 (2014).

6. Dube, F. & Stolpe, N. B. SOM and Biomass C Stocks in Degraded and Undisturbed Andean and Coastal *Nothofagus* Forests of Southwestern South America. *Forests* 7, 320, doi:10.3390/f7120320 (2016).

7. Peri, P. L., Gargaglione, V., Pastur, G. M. N. & Lencinas, M. A. V. Carbon accumulation along a stand development sequence of *Nothofagus antarctica* forests across a gradient in site quality in Southern Patagonia. *Forest Ecol. Manag.* **260**, 229–237 (2010).

8. Matsuzaki, E., Sanborn, P., Fredeen, A. L., Shaw, C. H. & Hawkins, C. Carbon stocks in managed and unmanaged old-growth western redcedar and western hemlock stands of Canada's inland temperate rainforests. *Forest Ecol. Manag.* **297**, 108–119 (2013).

9. Carmona, M. R., Armesto, J. J., Aravena, J. C. & Pérez, C. A. Coarse woody debris biomass in successional and primary temperate forests in Chiloé Island, Chile. *Forest Ecol. Manag.* **164**, 265–275 (2002).

10. Coomes, D. A., Holdaway, R. J., Kobe, R. K., Lines, E. R. & Allen, R.B. A general integrative framework for modelling woody biomass production and carbon sequestration rates in forests. *J. Ecol.* **100**, 42–64 (2011).

11. Davis, M. R., Allen, R. B. & Clinton, P. W. Carbon storage along a stand development sequence in a New Zealand *Nothofagus* forest. *Forest Ecol. Manag.* **177**, 313–321 (2002).

12. Schlegel, B. C. & Donoso, P. J. Effects of forest type and stand structure on coarse woody debris in old-growth rainforests in the Valdivian Andes, south-central Chile. *Forest Ecol. Manag.* **255**, 1906–1914 (2008).

13. Gutiérrez, A. G. & Huth, A. Successional stages of primary temperate rainforests of Chiloé Island, Chile. *Persp. Plant Ecol., Evol. Sys.* **14**, 243–256 (2012).

14. Swanson, F. J. & Major, J. J. in *Ecological Responses to the 1980 Eruption of Mount St. Helens* (eds Dale, V. H., Swanson, F. J. & Crisafulli, C. M.) 27–44 (Springer, 2005).

15. Frith, N.V. et al. Carbon export from mountain forests enhanced by earthquake-triggered landslides over millennia. *Nature Geosci.* **11**, 772–776 (2018).